10.3217/978-3-99161-093-9-030

Riemannian approaches for ECoG-based Motor Imagery BCI decoding using spatial covariance matrices : a comparative study

M. Etienne [1], F. Martel [1], S. Bonnet [2], T. Aksenova [1]

[1]Univ. Grenoble Alpes, CEA, LETI, Clinatec, Grenoble, France
[2]Univ. Grenoble Alpes, CEA, LETI, Grenoble, France

E-mail: mathis.etienne@cea.fr

ABSTRACT:
Symmetric positive definite (SPD) covariance matrices have demonstrated strong potential for motor imagery (MI) decoding in EEG-based brain-computer interfaces (BCIs), yet their application to electrocorticography (ECoG) data remains largely unexplored.
In this study, we evaluate and compare multiple classification approaches leveraging the Riemannian geometry of SPD matrices for ECoG-based MI decoding, across two paradigms: upper limb (3-class) and lower limb (3-class) motor imagery. Spatial covariance matrices were estimated from signals filtered in two task-specific frequency bands and used as input features. Three families of classifiers were compared: tangent space mapping (TSM) combined with machine learning models (LR, LDA, RSW-NPLS, LightGBM) and a multilayer perceptron (MLP); classifiers operating directly on the Riemannian manifold (MDM, FgMDM); and an SPD-aware neural network (SPDNetBN). Models were trained and tested offline on data from two implanted patients using lag-corrected balanced accuracy as the performance metric. FgMDM and TSM+RSWPLS achieved the highest performance for the upper limb paradigm (up to 91.6% and 89.5%, respectively), while SPDNetBN demonstrated superior accuracy for the lower limb paradigm (up to 69.4%).

INTRODUCTION

A brain-computer interface (BCI) is a technology that translates a person's brain activity into commands that control external devices. It typically consists of sensors that record neural activity, a signal processing pipeline to decode the recorded signal (often called a decoder), and one or more actuators. BCIs hold significant promise for assistive and rehabilitation applications, particularly for individuals with severe motor disabilities or neurodegenerative diseases..

Electroencephalography (EEG) remains the most widely used recording method for BCIs because of its low cost, non-invasive nature and ease of use. In contrast, electrocorticography (ECoG), although more invasive, offers superior spatial resolution, higher signal-to-noise ratio, broader frequency coverage, and greater long-term signal stability. These advantages make ECoG particularly well suited for decoding complex motor imagery tasks, including fine movements of the upper and lower limbs [1, 2].

Traditionally, BCI decoding pipelines incorporate a feature extraction step that provides discriminative information to downstream classifiers. Commonly used features include, among others, band-power estimates in sensorimotor rhythms (e.g., μ, β and γ bands), event-related desynchronization/synchronization (ERD/ERS) patterns or time–frequency representations.

Since 2010, a new family of features based on symmetric positive definite (SPD) covariance matrices has gained prominence in EEG-based motor imagery (MI) classification, as they naturally capture spatial correlation patterns across channels [3]. Importantly, SPD matrices lie on a Riemannian manifold endowed with a non-Euclidean geometry, which should be taken into account during decoder learning. This geometric perspective has led to the development of dedicated classification algorithms that respect the manifold structure, demonstrating improved performance over conventional Euclidean methods [4].

Several methodological approaches exist for leveraging this Riemannian geometry: classifiers may operate directly on the manifold using appropriate geometric metrics, SPD matrices can be projected into a tangent space, where conventional machine learning algorithms or neural networks can be applied, or specialized neural network architectures can be designed to preserve manifold structure throughout processing.

While SPD matrix-based approaches have become increasingly popular for EEG, their application to ECoG remains largely unexplored. Unlike EEG, ECoG electrodes are placed directly on the cortical surface, providing more localized coverage and closer proximity to neural sources. These differences in spatial scale may influence the structure of SPD matrices and, consequently, the effectiveness of Riemannian-based analyses.

To date, only methods employing tangent space mapping (TSM) have been evaluated with ECoG data. These include covariance matrices projected via TSM and subsequently decoded with machine learning models such as logistic regression [5], neural networks (LSTM) [6], and approaches combining TSM-projected covariance matrices with more conventional spectro-temporal features where decoding is performed by classical machine learn-

 10.3217/978-3-99161-093-9-030

ing models (linear model, Random Forest, Support Vector Machines) or gradient boosting trees (lightGBM) [7]. The tasks addressed in these studies range from hand motor imagery [5] (tetraplegic patient) to actual hand movements [6] (able-bodied monkeys) and fingers movements [7] (able-bodied humans). Manifold-based models and SPD neural network architecture have yet to be explored for ECoG data.

To address this gap, we evaluate several of these approaches on ECoG data acquired during upper and lower limb motor imagery tasks performed by one paraplegic and one tetraplegic patient. We investigate three categories of methods: [i] tangent space mapping (TSM) combined with conventional machine learning classifiers (logistic regression (LR), linear discriminant analysis (LDA)), N-way partial least squares (NPLS), and gradient boosted trees (lightGBM)[7]; [ii] classifiers operating directly on the Riemannian manifold (Minimum Distance to Mean (MDM) and Fisher Geodesic MDM (Fg-MDM)); and [iii] neural network approaches, including both SPD-aware architectures (SPDNetBN) and a conventional network applied to tangent space projections (multilayer perceptron (MLP)). To do so, we compared the decoding performance of each approach using lag-corrected balanced accuracy across two datasets (upper limb and lower limb conditions), each comprising three MI states.

MATERIALS AND METHODS

Experimental data:

Data were collected from two subjects: one tetraplegic (S1) enrolled in the BCI & Tetraplegia clinical trial (ClinicalTrials.gov identifier: NCT02550522), and one paraplegic (S2) enrolled in the STIMO-BSI clinical trial (ClinicalTrials.gov identifier: NCT04632290). Both participants were implanted with two wireless WIMAGINE devices [1] positioned over sensorimotor cortices for long-term epidural electrocorticography (ECoG) recording. Additionally, S2 received an epidural electrical stimulation (EES) pulse generator targeting spinal cord regions involved in leg movement control [2].

Participants performed asynchronous motor imagery tasks during experimental sessions: upper limb movements for S1 (3 classes : idle, left hand translation, right hand translation) and walking for S2 (3 classes : idle, left hip, right hip). Based on the decoder predictions, S1 could control a two-arm neuroprosthetic exoskeleton. S2 could control gait movements through stimulation of the nerves originating in the spinal cord using epidural stimulation. Two excerpts from the recording of cues and online predictions are shown in Fig. 1. The WIMAGINE devices recorded ECoG signals at 585 Hz sampling rate.

Sessions used for training and testing are resumed in Table 1.

Feature extraction:

We employed spatial covariance estimators, which are widely established in the BCI literature [4]. Covariance matrices were computed from filtered ECoG signals to capture spatial correlation patterns across distinct frequency bands. For each trial, signals from selected electrodes were bandpass-filtered using two fifth-order Butterworth filters to isolate frequency-specific neural activity.

Table 1: Summary of sessions used for training and testing (number of classes, number of sessions and duration).

Paradigm	Classes	Train sessions	Test sessions
S1 (upper limb)	3	3 (191 min)	6 (242 min)
S2 (lower limb)	3	4 (15 min)	21 (125 min)

Covariance matrix estimation For each trial and spatial configuration, the spatial covariance matrix was estimated separately for each frequency band. Given the filtered signals $\mathbf{X}_k \in \mathbb{R}^{n_c \times T}$ for band $k \in \{1,2\}$, where n_c denotes the number of electrodes and T the number of time samples, the block covariance matrix $\mathbf{C} \in \mathbb{R}^{m \times m}$ with $m = 2n_c$ is defined as:

$$\mathbf{C} = \begin{pmatrix} \mathbf{C}_1 & \mathbf{0} \\ \mathbf{0} & \mathbf{C}_2 \end{pmatrix}. \tag{1}$$

Each block $\mathbf{C}_k$ is estimated using the Ledoit-Wolf shrinkage estimator [8], which provides a regularized estimate balancing the sample covariance with a scaled identity target:

$$\mathbf{C}_k = (1-\rho_k)\mathbf{S}_k + \rho_k \frac{\mathrm{tr}(\mathbf{S}_k)}{n_c}\mathbf{I}_{n_c}, \tag{2}$$

where $\mathbf{S}_k = \frac{1}{T-1}\mathbf{X}_k\mathbf{X}_k^T$ is the sample covariance matrix for band k, $\mathbf{I}_{n_c}$ is the identity matrix, and $\rho_k \in [0,1]$ is the shrinkage parameter estimated as described in [8]. We also investigated a spatial frequency covariance estimate computed across all m channels jointly, allowing non-zero inter-frequency covariance between the two bands.

Number of time samples per trial was fixed at $T = 590$ (1 second of data) for S1 and $T = 236$ (400 ms of data) for S2, based on previous studies [1, 2].

Classification:

Importantly, covariance matrices yield SPD matrices that lie on a differentiable Riemannian manifold, where standard Euclidean operations such as arithmetic mean and Euclidean metrics are inappropriate and can lead to suboptimal classification performance [9].

There are three ways to handle this, taking into account the geometry of the covariance matrix space: use classification algorithms that operate directly on the Riemannian manifold, project the covariance matrices onto an Euclidian tangent space in order to apply conventional classification algorithms, or design specific neural networks that manipulate SPD matrices.

Classification within the Riemannian manifold Riemannian manifold geometry-based classifiers operate directly on the manifold of Symmetric Positive Definite (SPD) matrices by leveraging Riemannian metrics to compute distances and class means. These include the

10.3217/978-3-99161-093-9-030

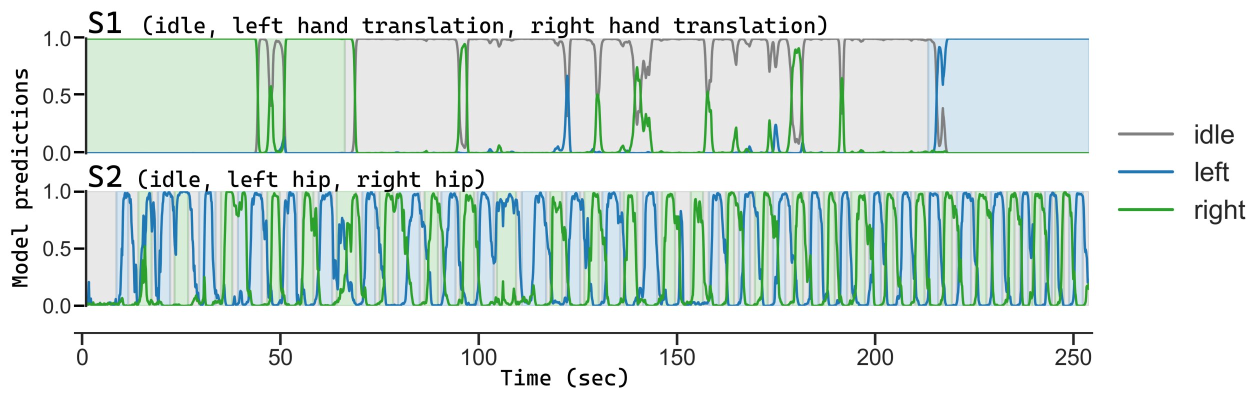

Figure 1: Online prediction excerpt from two sessions (S1, top; S2, bottom). The background shading indicates the desired cue, while the lines represent the model predictions. During each motor cue, S1 performed continuous 3D movement tasks with an exoskeleton [1]. The duration of the cues is therefore longer. For clarity, the display of the idle prediction is disabled for S2.

Minimum Distance to Mean (MDM) and its variant, the Fisher Geodesic MDM (FgMDM) [3]. These classifiers have been shown to be particularly effective for BCI applications, as they inherently respect the geometric structure of covariance matrices [4]. The distance employed in this study is the Affine Invariant Riemannian Metric (AIRM) distance, which operates on the manifold of symmetric positive definite (SPD) matrices. The AIRM distance between two SPD matrices $\mathbf{C}_1$ and $\mathbf{C}_2$ is defined as:

$$\delta_R(\mathbf{C}_1, \mathbf{C}_2) = \left\| \operatorname{logm}(\mathbf{C}_1^{-1/2}\mathbf{C}_2\mathbf{C}_1^{-1/2}) \right\|_F, \qquad (3)$$

where $\|\cdot\|_F$ denotes the Frobenius norm and $\operatorname{logm}(\cdot)$ represents the matrix logarithm.
The MDM classifier assigns each trial to the class whose geometric mean is closest in terms of AIRM distance.
The geometric mean $\overline{\mathbf{C}}$ of a set of SPD matrices $\{\mathbf{C}_n\}_{n=1}^N$ is computed by minimizing the sum of squared Riemannian distances :

$$\overline{\mathbf{C}} = \arg\min_{\mathbf{C}} \sigma(\mathbf{C}), \quad \sigma(\mathbf{C}) = \sum_{n=1}^{N} \delta_R^2(\mathbf{C}, \mathbf{C}_n) \qquad (4)$$

Since no closed-form solution exists, the geometric mean is estimated iteratively [9]. An example of the geometric mean for S2 is given in Figure 2.

Classification on tangent space To enable the use of conventional machine learning algorithms that operate in Euclidean space, Tangent Space Mapping (TSM) was applied [9]. TSM projects covariance matrices from the manifold of SPD matrices onto a tangent space of the manifold at a reference point, typically chosen as the geometric mean of the training covariances.
The tangent space feature vector $\mathbf{t}_i$ for a given covariance matrix $\mathbf{C}_i$ is obtained by computing the logarithmic map at the reference point:

$$\mathbf{t}_i = \operatorname{vech}\left[\operatorname{logm}\left(\overline{\mathbf{C}}^{-1/2}\mathbf{C}_i\overline{\mathbf{C}}^{-1/2}\right)\right], \qquad (5)$$

where $\operatorname{vech}(\cdot)$ half-vectorizes the upper triangular part of the symmetric matrix into a feature vector of dimension $m(m+1)/2$, preserving ℓ_2 norm.
In this study, multiple state-of-the-art classifiers were applied to the tangent space features. Classical machine learning approaches included Linear Discriminant Analysis (LDA) and Logistic Regression (LR), an effective PLS model for classifying ECoG data in real time (Recursive Sample Weighted – N-way Partial Least Squares (RSW-NPLS) [10]), and an ensemble of gradient boosting trees (lightGBM) [7]. A multilayer perceptron (MLP) with two hidden layers (32 and 16 units) was also evaluated as a simple deep learning baseline. Hyperparameters were tuned on a validation set comprising 20% of the training data.

Classification with SPD Neural Networks Additionally, we investigated SPDNet [11] with Riemannian batch normalization (BN) [12], a specialized neural network architecture designed to operate directly on SPD matrices. SPDNet incorporates Riemannian geometry throughout its layers, utilizing bilinear mapping and rectification operations that preserve the manifold structure. The network concludes with a tangent space mapping layer using the identity matrix as the reference point, projecting features into Euclidean space for final classification. This approach combines the geometric awareness of Riemannian methods with the representational capacity and nonlinearity of deep learning.

Hidden Markov Model A Hidden Markov Model (HMM) was applied to all the classifier outputs to improve prediction robustness and temporal consistency [1].

Feature configuration:

Frequency band selection Frequency band selection was guided by analysis of class distinctiveness across the spectrum [13]. This approach quantifies the separability between motor imagery classes by computing the Riemannian class distinctiveness for each frequency

10.3217/978-3-99161-093-9-030

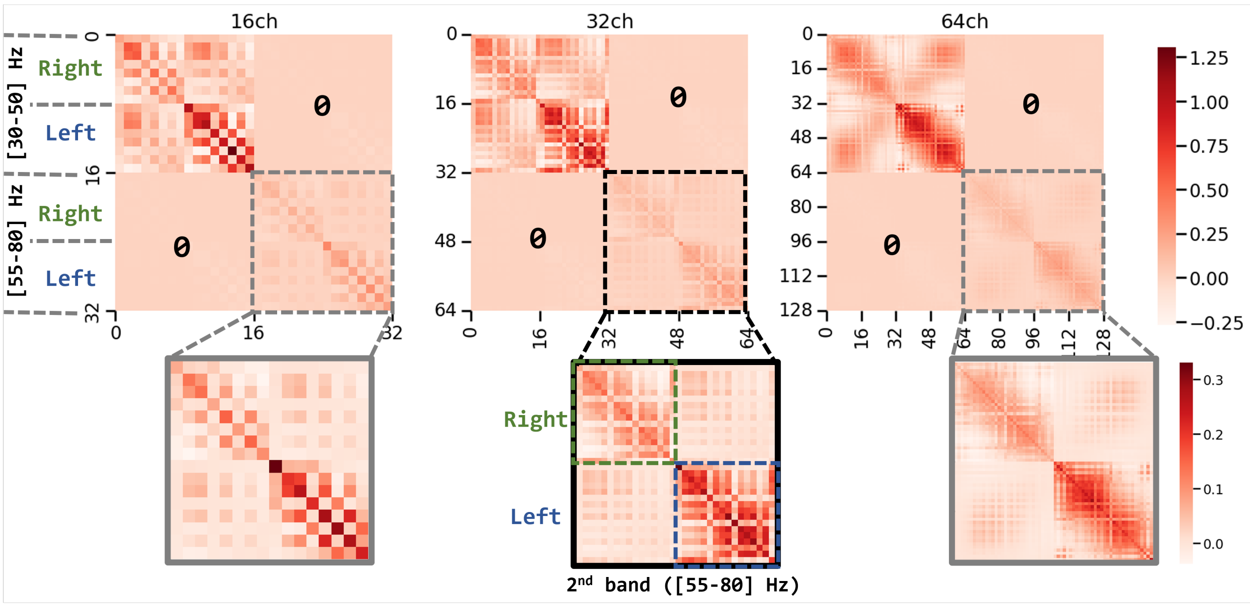

Figure 2: Mean covariance matrices from S2 training data (all classes) for 16, 32, and 64 channels. Each block matrix shows intra-band covariance (top-left: low-frequency; bottom-right: high-frequency). Within each diagonal block: right implant (top-left), left implant (bottom-right), and inter-implant covariances (top-right/bottom-left).

band, identifying bands where spatial covariance matrices (SCMs) differ most significantly between conditions. For a given frequency band f_i, the class distinctiveness between two classes A and B is defined as:

$$\text{classDis}(f_i) = \frac{\delta_R(\overline{\mathbf{C}}_A(f_i), \overline{\mathbf{C}}_B(f_i))}{\sigma_A(f_i) + \sigma_B(f_i)}, \tag{6}$$

where $\overline{\mathbf{C}}_A(f_i)$ and $\overline{\mathbf{C}}_B(f_i)$ are the Riemannian means of the SCMs computed from signals band-pass filtered in the frequency band $[f_i - 5\text{ Hz}, f_i + 5\text{ Hz}]$, for classes A (resting state) and B (active state, motor classes combined), respectively. The term $\delta_R(\cdot, \cdot)$ denotes the AIRM distance (Eq. 3), while $\sigma_A(f_i)$ and $\sigma_B(f_i)$ correspond to the Riemannian mean absolute deviation within each class and frequency band (defined in Eq. 4).

Higher values of classDis(f_i) indicate greater discriminability between classes at specific frequency bands.

Based on the class distinctiveness analysis (Figure 3), conducted using only two training sessions, two broader frequency bands were selected for each subject : $[10, 45]$ Hz and $[55, 75]$ Hz for S1, $[30, 50]$ Hz and $[55, 80]$ Hz for S2. These bands are selected for their discriminability and coherence with event-related desynchronization (ERD) below 50 Hz and event-related synchronization (ERS) above 50 Hz observed in ECoG data [14].

Spatial electrode configurations Each WIMAGINE implant contains 64 electrodes arranged in an 8x8 grid, but only 32 of them were activated during the recording period used in this study, due to hardware limitations. Three spatial configurations were evaluated to assess the trade-off between spatial resolution and feature dimension : full electrode coverage with 64 channels (32 per implant) and spatially subsampled montages with 32 and 16 channels (Figure 4). The electrode subsets were selected randomly while preserving spatial distribution (reduction performed in areas of 4 close neighbours, 1 over 4 for 16, 2 over 4 for 32). The results are averaged over 50 sub-selections per configuration.

Performance evaluation:

We evaluated decoding performance using lag-corrected balanced accuracy (lcBA). For each session, we estimated the latency as the lag maximizing the cross-correlation between labels and predictions, averaged across motor states. Predictions were then shifted by this lag before computing balanced accuracy (average per-class recall).

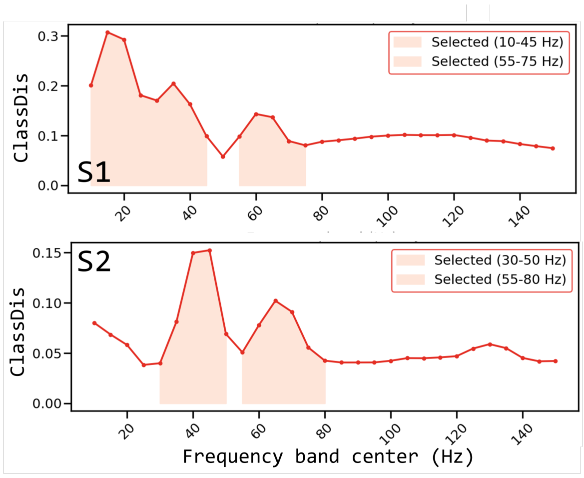

Figure 3: Class distinctiveness across frequencies for S1 and S2 training data.

 10.3217/978-3-99161-093-9-030

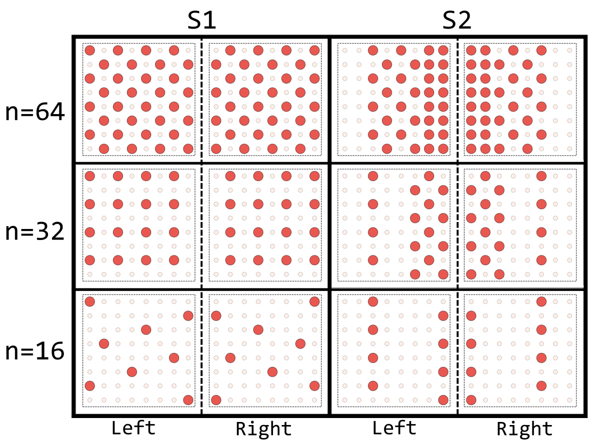

Figure 4: Example of electrode configurations with 64, 32, and 16 channels. Both participants were implanted with two 50 mm WIMAGINE implants (right and left hemispheres), each containing 64 recording electrodes. Red circles indicate active electrodes.

RESULTS

Decoding performance was evaluated using lag-corrected balanced accuracy across models, channel numbers (16, 32, and 64), and tasks (upper and lower limb motor imagery), as summarized in Table 2.

For S1 (upper limbs), the highest performance at 16 channels was obtained with TSM+RSWPLS (85.4% $\pm$ 3.6%), closely followed by FgMDM (85.1% $\pm$ 3.3%). At 32 and 64 channels, FgMDM achieved the best results (88.8% $\pm$ 2.4% and 91.6% $\pm$ 1.7%, respectively), with TSM+RSWPLS remaining competitive (88.3% $\pm$ 2.8% and 89.5% $\pm$ 2.0%). Across all channel configurations, TSM+RSWPLS consistently outperformed other tangent-space-based classifiers (TSM+LR, TSM+LDA, TSM+LightGBM, and TSM+MLP). MDM yielded substantially lower accuracies (58.2%–58.6%). SPDNetBN achieved moderate results, reaching 84.1% $\pm$ 1.8% at 64 channels, but remained below FgMDM and TSM+RSWPLS for all configurations.

For S2 (lower limbs), TSM+RSWPLS achieved the highest accuracy at 16 channels (68.9% $\pm$ 6.3%), closely followed by SPDNetBN (68.8% $\pm$ 6.0%) and FgMDM (68.7% $\pm$ 6.3%). Increasing the number of channels did not lead to systematic improvements across models. SPDNetBN yielded the best performance at both 32 and 64 channels (69.4% $\pm$ 5.3% and 68.1% $\pm$ 4.3%, respectively), and was the only model to remain stable with increasing channel count. TSM+RSWPLS decreased to 67.2% $\pm$ 5.7% and 64.9% $\pm$ 5.2%. Other tangent-space-based classifiers and manifold classifiers remained less performing and decreased similarly with the increasing number of electrodes. TSM+LightGBM and TSM+MLP showed relatively stable but lower performances across channel counts, with best results of 60.2% $\pm$ 4.9% and 60.6% $\pm$ 5.0% at 32 electrodes, respectively.

The spatio-frequency covariance (with inter-frequency covariance) performance was largely comparable, with an average difference of -0.5% across all classifiers and channel counts.

DISCUSSION

This offline study provides a comparative evaluation of tangent space mapping (TSM), intrinsic Riemannian classifiers, and SPD-aware neural networks for ECoG motor imagery decoding. The three types of classifiers showed strong potential.

For the lower limbs paradigm, some models show declining performance with increasing electrodes number, likely due to the task's simplicity rendering additional spatial information redundant. This is not observed for the upper limb paradigm. Indeed, during cue periods, the patient performed motor imagery tasks for continuous hand movement (3D). This may have complicated the classification, where the addition of electrodes should be beneficial.

The lower performance observed for paradigm S2 (lower limbs) compared to S1 (upper limb) is likely attributable to task duration. In S2, gait tasks alternated every two to three seconds, whereas S1 maintained a single state for over 30 seconds on average. Since transition periods are inherently harder to classify, more frequent transitions in S2 reduce overall performance.

In practice, compatibility with incremental and online learning is essential, as it enables closed-loop training in which patients receive real-time feedback during learning. This is achievable with some of the models evaluated here, but with adjustments (Table 3).

Furthermore, combining SPD matrices projected into tangent space with other types of features (e.g. time-frequency), here referred to as hybrid features, has been shown to improve decoding performance [7]. However, this is not possible natively for classifiers on the Riemannian manifold and for neural networks designed for SPD matrices (Table 3). These considerations should guide model selection. Among the evaluated approaches, RSWNPLS offers the best trade-off across these criteria.

Limitations:

In this study, only one covariance matrix is used as feature. This was chosen for compatibility with MDM, FgMDM and SPDNetBN. Only two frequency bands were selected in order to limit the feature size. To improve performance, one can consider increasing the number of matrices and/or the number of frequencies studied. In this case, more complex architectures can be used, such as graph neural networks on SPD manifolds. Other types of matrices, such as cross-frequency covariance matrices, may also be considered [6].

Furthermore, this study was conducted on only two patients. Increasing the amount of data will enable the robustness of the proposed models to be validated.

Finally this work is an offline study. It therefore lacks the human factor, which could influence the result (closed-loop BCI). An online study of these models for real-time experiments is needed to confirm the observed results.

 10.3217/978-3-99161-093-9-030

Table 2: Lag-corrected balanced accuracy (mean ± std) across models, channel numbers, and tasks (in %).

Participant	Channels	TSM+RSWPLS	TSM+LR	TSM+LDA	TSM + LightGBM	TSM+MLP	MDM	FgMDM	SPDNetBN
S1 (upper limbs)	16 (x50)	**85.4 ± 3.6**	79.0 ± 2.6	78.9 ± 2.3	80.4 ± 1.5	80.9 ± 2.2	58.3 ± 3.7	85.1 ± 3.3	79.7 ± 2.4
	32 (x50)	88.3 ± 2.8	81.3 ± 2.0	82.2 ± 1.8	82.5 ± 1.4	82.0 ± 2.1	58.6 ± 3.2	**88.8 ± 2.4**	82.7 ± 2.1
	64 (x1)	89.5 ± 2.0	81.1 ± 1.6	81.8 ± 1.5	83.7 ± 1.1	81.8 ± 1.7	58.2 ± 3.2	**91.6 ± 1.7**	84.1 ± 1.8
S2 (lower limbs)	16 (x50)	**68.9 ± 6.3**	65.5 ± 5.5	65.2 ± 5.2	59.2 ± 5.3	60.2 ± 5.4	60.7 ± 10.0	68.7 ± 6.3	68.8 ± 6.0
	32 (x50)	67.2 ± 5.7	62.5 ± 4.9	60.5 ± 4.3	60.2 ± 4.9	60.6 ± 5.0	58.1 ± 9.7	65.0 ± 7.0	**69.4 ± 5.3**
	64 (x1)	64.9 ± 5.2	57.9 ± 3.9	50.3 ± 2.7	59.8 ± 5.2	60.3 ± 4.4	53.7 ± 8.4	60.3 ± 7.4	**68.1 ± 4.3**

Table 3: Model compatibility with online/incremental learning (streaming updates without full data storage, at the cost of adaptations/approximations) and hybrid features.

Model compatibility with	Streaming / Incremental Learning	Hybrid Features
TSM+RSWPLS	Yes	Yes
TSM+LR	Yes	Yes
TSM+LDA	Yes	Yes
TSM+LightGBM	No	Yes
MDM	Yes	No
FgMDM	Limited	No
SPDNetBN	No	No
TSM+MLP	No	Yes

CONCLUSION

This study compare mutliple classification techniques leveraging the geometry of SPD-based features for ECoG motor imagery BCI. The features used are spatial covariance matrices of signals from two frequency bands.
Machine learning classifiers applied after tangent space mapping, classifiers operating within the manifold, and neural networks designed for SPD matrices were compared. To this end, the models were trained and tested offline on two paradigms : upper limb and lower limb motor imagery classification. All three approaches yielded satisfactory results on at least one of the two paradigms.
Additional experiments should be conducted to confirm these results, with more participants performing other motor tasks. Then the models will need to be adapted, if possible, to function online for closed-loop learning.

ACKNOWLEDGMENT

The authors would like to thank all the members of the BCI project at Clinatec (CEA-Leti, Grenoble Alpes University Hospital, and University Grenoble Alpes), composed of the multidisciplinary technical and clinical teams. We also thank all the members of the NeuroRestore team for conducting the STIMO-BSI clinical trial and collecting the data used in this study. This study was funded by CEA (CFR and Bluesky-EXPLORE+).

REFERENCES

[1] Benabid AL et al. An exoskeleton controlled by an epidural wireless brain–machine interface in a tetraplegic patient: A proof-of-concept demonstration. The Lancet Neurology. 2019;18(12):1112–1122.
[2] Lorach H et al. Walking naturally after spinal cord injury using a brain–spine interface. Nature. 2023;618(7963):126–133.
[3] Barachant A, Bonnet S, Congedo M, Jutten C. Riemannian geometry applied to BCI classification. In: LVA/ICA 2010 - 9th International Conference on Latent Variable Analysis and Signal Separation. Springer: Saint-Malo, France, Sep. 2010, 629–636.
[4] Lotte F et al. A Review of Classification Algorithms for EEG-based Brain-Computer Interfaces: A 10-year Update. Journal of Neural Engineering. 2018;15.
[5] Liu D et al. "Reclaiming Hand Functions after Complete Spinal Cord Injury with Epidural Brain-Computer Interface." Accessed: May 13, 2025. [Online]. Available: https://www.medrxiv.org/content/10.1101/2024.09.05.24313041v6 preprint.
[6] Eyvazpour R, Farrokhi B, Erfanian A. A general model based on Riemannian manifold for stable decoding movement trajectory from ECoG signals. iScience. 2026;29(2):114521.
[7] Yao L, Zhu B, Shoaran M. Fast and accurate decoding of finger movements from ECoG through Riemannian features and modern machine learning techniques. Journal of Neural Engineering. 2022;19(1):016037.
[8] Ledoit O, Wolf M. A well-conditioned estimator for large-dimensional covariance matrices. Journal of Multivariate Analysis. 2004;88(2):365–411.
[9] Barachant A, Bonnet S, Congedo M, Jutten C. Classification of covariance matrices using a Riemannian-based kernel for BCI applications. Neurocomputing. 2013;112:172–178.
[10] Souriau R, Martel F, Aksenova T. Recursive sample weighted – N-way partial least squares for brain-computer interface decoder online learning with class imbalance. Biomedical Signal Processing and Control. 2026;113:109025.
[11] Huang Z, Gool LV. A Riemannian Network for SPD Matrix Learning. Proceedings of the AAAI Conference on Artificial Intelligence. 2017;31(1).
[12] Brooks D, Schwander O, Barbaresco F, Schneider JY, Cord M. Riemannian batch normalization for SPD neural networks. In: Advances in Neural Information Processing Systems. Curran Associates, Inc., 2019.
[13] Yamamoto MS, Lotte F, Yger F, Chevallier S. Class-distinctiveness-based frequency band selection on the Riemannian manifold for oscillatory activity-based BCIs: Preliminary results. In: 2022 44th Annual International Conference of the IEEE Engineering in Medicine & Biology Society (EMBC). Jul. 2022, 3690–3693.
[14] Moly A et al. An adaptive closed-loop ECoG decoder for long-term and stable bimanual control of an exoskeleton by a tetraplegic. Journal of Neural Engineering. 2022;19(2):026021.